SCIENTIFIC REPORTS

OPEN

Experimental proof of the reciprocal relation between spin Peltier and spin Seebeck effects in a bulk YIG/Pt bilayer

Received: 4 October 2018
Accepted: 8 January 2019
Published online: 14 February 2019

Alessandro Sola[1], Vittorio Basso[1], Michaela Kuepferling[1], Carsten Dubs[2] & Massimo Pasquale[1]

We verify for the first time the reciprocal relation between the spin Peltier and spin Seebeck effects in a bulk YIG/Pt bilayer. Both experiments are performed on the same YIG/Pt device by a setup able to accurately determine heat currents and to separate the spin Peltier heat from the Joule heat background. The sample-specific value for the characteristics of both effects measured on the present YIG/Pt bilayer is $(6.2 \pm 0.4) \times 10^{-3}$ KA^{-1}. In the paper we also discuss the relation of both effects with the intrinsic and extrinsic parameters of YIG and Pt and we envisage possible strategies to optimize spin Peltier refrigeration.

The reciprocal relations of thermodynamics are a fundamental tool to analyze and understand the physics of transport phenomena[1]. Since the beginning of the 19th century it was clear to Jean Charles Athanase Peltier and later demonstrated by Lord Kelvin, that for a material at a given absolute temperature T a relation exists between the Seebeck coefficient ε (given by the ratio between the measured electromotive force and the applied temperature difference) and the Peltier coefficient $\prod$ (the ratio between the measured heat current and the applied electric current): $\prod = \varepsilon T$[2,3]. This remarkable reciprocity was later found to be part of a wider set of relations, as theoretically demonstrated by Onsager under the assumption of the reversibility of the microscopic physical processes governing macroscopic non-equilibrium thermodynamic effects[4].

Reciprocal relations can also be used to analyze transport phenomena which involve not only the electric charge and the heat, but also the spin. Spincaloritronic phenomena[5–7] can provide additional tools to the field of spintronics, envisioned to be a faster and lower energy consuming alternative to classical electronics[8]. One of the key building blocks for "spintronic circuits" is the spin battery, a device which can drive a spin current into an external circuit. Spin batteries are fundamental for spintronic devices and may be developed exploiting spincaloritronic effects[9]. Spincaloritronic devices may also be used in the development of novel thermoelectric heaters/coolers operating at the microscale[10,11]. The idea of a reciprocity between heat and spin was initially proposed and proven for metals where the spin current is carried by electrons[12], but such a reciprocal relation cannot be easily proven in the case of ferrimagnetic insulators where the spin current is carried by thermally excited spin waves[13]. A typical device, where spincaloritronic effects are found and can be exploited for experiments, is a bilayer made of a ferrimagnetic insulator (e.g. yttrium iron garnet, YIG) and a non magnetic metal with a strong spin-orbit coupling (e.g. platinum, Pt)[14]. In these devices the spin current is generated longitudinally (along the x axis), normal to the film surface.

In the case of devices which exhibit the spin Peltier effect (SPE) a longitudinal (x axis) heat current is generated, caused by the flow of a transverse (y axis) electric current in the Pt layer[13]. Conversely, in the case of the spin Seebeck effect (SSE) a transverse (y axis) electric voltage is generated in the Pt layer and caused by the longitudinal temperature gradient parallel to the spin current (x axis)[15]. Although experimental evidence of both effects has been already obtained[16,17], the quantitative demonstration of their reciprocity and the connection with intrinsic properties of the layers, has yet to be proven[13,18–20]. To this end here we provide the first experimental evidence of the reciprocal relation between the thermal and the electric quantities associated to the SPE and the SSE in a bulk YIG/Pt bilayer. The relation for a YIG/Pt bilayer has the following form[21,22]

[1]Istituto Nazionale di Ricerca Metrologica, Strada delle Cacce 91, 10135, Torino, Italy. [2]INNOVENT e.V., Technologieentwicklung, Prüssingstrasse. 27B, 07745, Jena, Germany. Correspondence and requests for materials should be addressed to A.S. (email: a.sola@inrim.it)

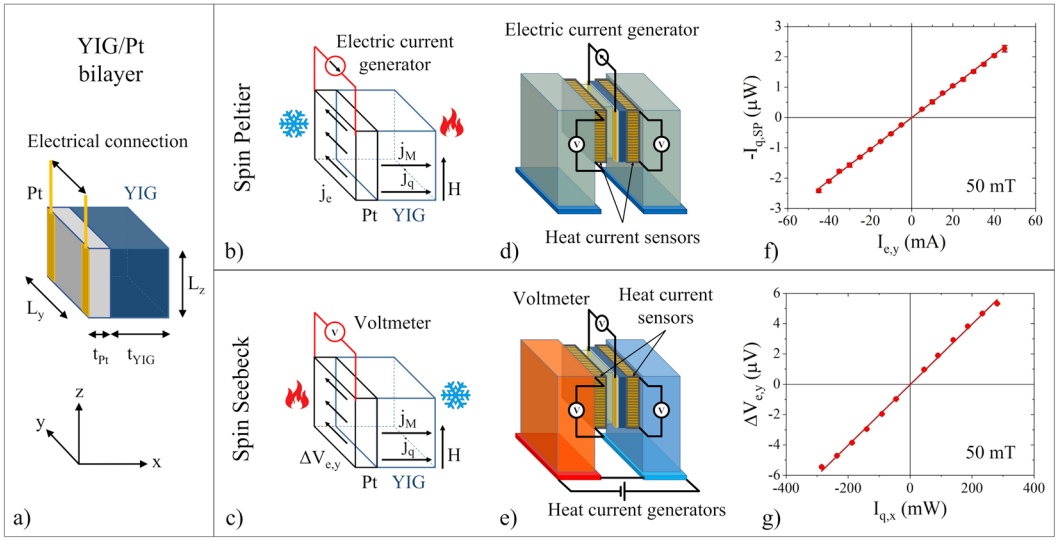

Figure 1. (**a**) Geometry of the YIG/Pt bilayer with $t_{YIG} = 0.545$ mm, $L_y = 4.95$ mm, $L_z = 3.91$ mm and $t_{Pt} = 5$ nm. (**b**,**c**) schemes of the device in the SPE and SSE configurations. Heat currents and magnetic moment currents are along x (longitudinal direction), electric effects are along y (transverse direction), the magnetic field and the magnetization are along z. (**d**,**e**) sketches of the experimental setup for SPE and SSE, respectively. (**f**) Experimental result of the SPE heat current, $-I_{q,SP}$, as function of the electric current $I_{e,y}$ at positive magnetic saturation. (**g**) Experimental result of the SSE voltage $\Delta V_{e,y}$ as function of the heat current $I_{q,x}$ at positive magnetic saturation.

$$\frac{-\Delta T_{SP,x}}{I_{e,y}} = \frac{\Delta V_{e,y}}{I_{q,x}} T \tag{1}$$

The left hand side of Eq. (1) refers to the SPE: ΔT_{SPx} is the temperature difference generated across the YIG layer as consequence of the electric current $I_{e,y}$ flowing in the Pt film. The right hand side of Eq. (1) refers to the SSE: $\Delta V_{e,y}$ is the voltage drop across the Pt film caused by the heat current $I_{q,x}$ flowing across the device and T is the average temperature of the YIG. The experiments are performed measuring the SPE and the SSE on the same YIG/Pt device. The experimental value which represents, within the uncertainty, both the SPE and the SSE response of the specific device is $(6.2 \pm 0.4) \times 10^{-3}$ KA^{-1}.

Results

Device geometry and measurement principle. The geometry of the bulk YIG/Pt bilayer is shown in Fig. 1a.

The device is composed of a bulk YIG parallelepiped with a thin film of Pt sputter deposited on one side. The temperature gradient $\nabla_x T$ and the heat current density $j_{q,x}$ are directed along the x axis. The electric voltage $\Delta V_{e,y}$ and the electric current density $j_{e,y}$ are directed along the y axis. The magnetic moment current density, j_M, is along the x direction and transports magnetic moments directed along the z direction. The magnetic field H and the magnetization M of the bulk-YIG are also directed along the z axis (Fig. 1b,c). The measurement setup for both SPE and SSE is shown in the sketches of Fig. 1c,e. The YIG/Pt device is sandwiched between two thermal reservoirs (held at T_h and T_c respectively) in order to form a closed thermal circuit. The temperature of the two reservoirs can be externally controlled and the two heat currents between the device and each of the reservoirs are measured simultaneously by sensitive heat flux detectors. The heat flux technique is chosen to avoid measurement uncertainties due to the hardly reproducible thermal contacts[23–26]. In order to minimize heat leakages in the thermal circuit, the whole setup is operated in vacuum. Technical, constructional and measurement details are reported in the Methods section.

Spin Peltier effect. In the SPE, an electric current $I_{e,y}$ flowing in the Pt layer generates a magnetic moment current j_M along the x direction as a result of the spin Hall effect[27]. The adjacent ferrimagnetic bulk YIG acts as a passive component and shows a longitudinal (x axis) heat current associated to the magnetic moment current injection[28–30]. The measured heat current is however also including the Joule heat contribution generated by the electric current flowing in the Pt layer. In order to separate the Joule and spin Peltier contributions, their intrinsic differences have to be exploited: the spin Peltier signal increases linearly with the $I_{e,y}$ current and changes sign when the magnetization (along the z axis) or the $I_{e,y}$ are inverted (odd parity), while Joule heating is proportional to $I_{e,y}^2$ and does not change sign under an inversion (even parity)[13,18].

The thermal problem of the SPE can be represented by the equivalent circuit of Fig. 2 (see also Supplementary material).

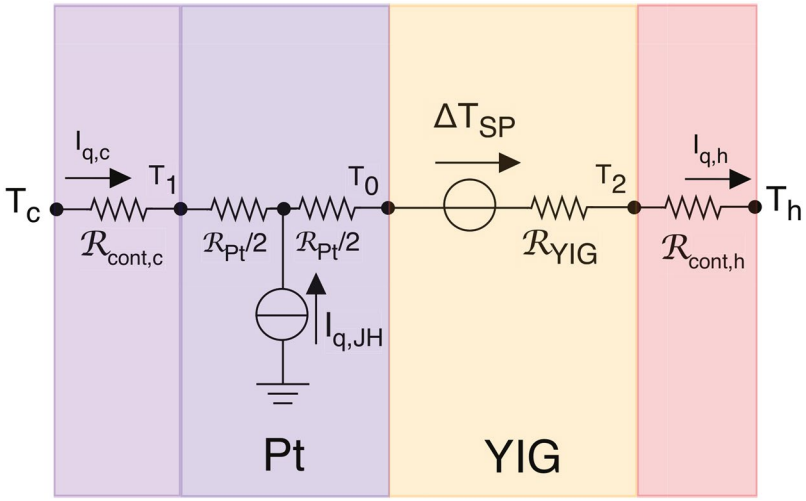

Figure 2. Equivalent thermal circuit of the SPE measurements of the YIG/Pt bilayer. The YIG layer is represented by the SPE generator, ΔT_{SP}, and by the thermal resistance $\mathcal{R}_{YIG}$. The Pt layer has a Joule heat current source, $I_{q,JH}$, and a thermal resistance $\mathcal{R}_{Pt}$. The circuit includes two thermal contact resistances $\mathcal{R}_{cont,c}$ and $\mathcal{R}_{cont,h}$ taking into account both the thermal resistance of the contacts and the presence of the heat flux sensors. The difference $I_{q,h} - I_{q,c} = I_{q,JH}$ provides the Joule heat. In isothermal conditions, with $T_h = T_c = T$, we have $\Delta T_{SP} = \mathcal{R} I_{q,s} + I_{q,JH}(\mathcal{R}_h - \mathcal{R}_c)/2$ where $\mathcal{R}_h = \mathcal{R}_{Pt}/2 + \mathcal{R}_{YIG} + \mathcal{R}_{cont,h}$, $\mathcal{R}_c = \mathcal{R}_{cont,c} + \mathcal{R}_{Pt}/2$, $I_{q,s} = (I_{q,h} + I_{q,c})/2$ is the half sum and $\mathcal{R} = \mathcal{R}_h + \mathcal{R}_c$ is the total resistance (see Supplementary material).

In adiabatic conditions the SPE corresponds to the direct measurement of ΔT_{SP}, the temperature difference generated between the two faces of the bulk YIG sample. Previous experimental works have succeeded to extract ΔT_{SP} out of the Joule heat component by using an AC technique[13,18]. Here, to test the reciprocal relation in a stationary state, we employ a DC technique in which we set isothermal conditions at the thermal baths, $T_h = T_c = T$, and measure simultaneously the two heat currents: $I_{q,c}$ and $I_{q,h}$. The difference of the heat flux signals $I_{q,h} - I_{q,c} = I_{q,JH}$ provides the Joule heat only (see Fig. 3a), while the half sum $I_{q,s} = (I_{q,h} + I_{q,c})/2$ contains the SPE signal (see Fig. 3b,c).

We first detect the SPE generated by setting a constant electric current (i.e. $I_{e,y} = 40$ mA, see Fig. 3b, orange points) and periodically inverting the magnetic field. The half sum signal $I_{q,s}$ has a change of $\pm 2 I_{q,SP}$ at each inversion. Equivalently, when the sign of the electric current in the Pt film is changed (i.e. $I_{e,y} = -40$ mA, Fig. 3b, purple points), a sign inversion of the change $\mp 2 I_{q,SP}$ occurs. The field inversion allows to detect the small contribution of the spin Peltier heat current (a few μW) superimposed to the Joule heating background (a few mW).

As a second step we measure the SPE signal $I_{q,s}$ at the constant magnetic field $\mu_0 H_s = +50$ mT while the applied current $I_{e,y} = \pm 40$ mA is periodically inverted, Fig. 3c, orange points. Conversely when we apply $\mu_0 H_s = -50$ mT and the applied current $I_{e,y} = \pm 40$ mA is inverted, we obtain the curve of Fig. 3c, purple points. The current inversion method provides the same results, within the uncertainty, as the magnetic field inversion one, provided one takes into account the presence of small spurious offset signals as discussed in the Methods section. This second method allows to detect the SPE signal as function of the applied magnetic field. Therefore it permits the determination of the hysteresis loop of YIG[31] (more details about this experiment are reported in Supplementary materials).

At the saturating magnetic field $\mu_0 H_s = +50$ mT, by applying different values of $I_{e,y}$ and by deriving the corresponding values of $-I_{q,SP}$ as shown in Fig. 3b,c, we are able to obtain the linear relation between the SPE heat current and the electric current data of Fig. 1f. By a linear fit we find

$$\frac{-I_{q,SP}}{I_{e,y}} = (5.1 \pm 0.3) \times 10^{-5}\ \mathrm{WA}^{-1} \tag{2}$$

The thermal resistance $\mathcal{R}$ of the whole stack consisting of sensors, sample and additional thermal contacts (e.g. thermal paste or thermally conducting layers) is experimentally measured by setting a heat current value and measuring the temperatures of the two thermal reservoirs by two thermocouples. The result is $\mathcal{R} = (119 \pm 2)\,\mathrm{KW}^{-1}$. With $\Delta T_{SP} = \mathcal{R} I_{q,SP}$, the measured spin Peltier coefficient is

$$\frac{-\Delta T_{SP}}{I_{e,y}} = (6.1 \pm 0.4) \times 10^{-3}\ \mathrm{KA}^{-1} \tag{3}$$

and since the current density flowing in the Pt film is $j_{e,y} = I_{e,y}/(t_{Pt} L_z)$ with $L_z = 3.9$ mm and $t_{Pt} = 5$ nm we are finally able to obtain the intrinsic SPE coefficient:

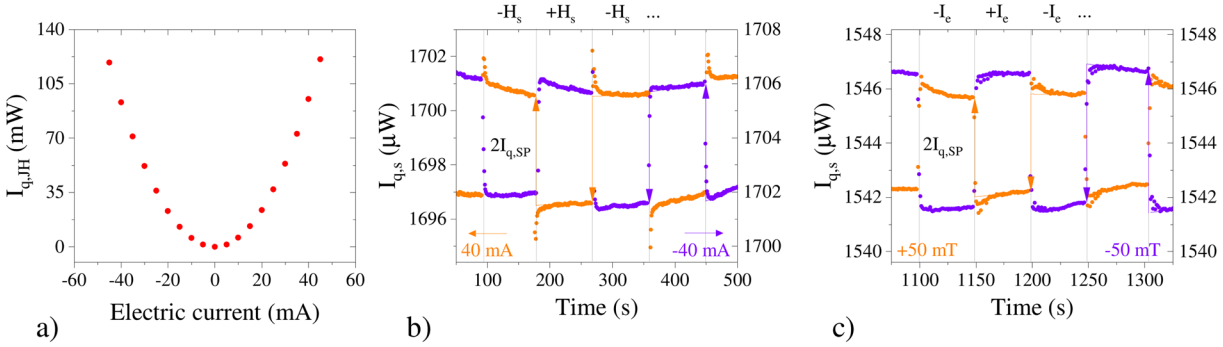

Figure 3. Heat current signals measured on the YIG/Pt bilayer during the SPE experiment. (**a**) Joule heat signal given by the difference $I_{q,JH} = I_{q,h} - I_{q,c}$. (**b**) SPE by magnetic field inversion. Half sum signal $I_{q,s} = (I_{q,h} + I_{q,c})/2$ caused by a rectangular waveform of the magnetic field $|\mu_0 H_s| = 50$ mT, for two steady values of electric current (±40 mA, orange/purple). (**c**) SPE by electric current inversion. $I_{q,s}$ caused by a rectangular waveform of the electric current $|I_{e,y}| = 40$ mA, for two steady values of magnetic field (±50 mT, orange/purple). In both cases the spin Peltier signal $I_{q,SP}$ is obtained as half of the variation at the inversion $I_{q,SP} = \Delta I_{q,s}/2$. The variation $\Delta I_{q,s}$ is taken at the inversion instant and is computed from the extrapolation of the linear fit taken a few seconds after the inversion. This method permits to avoid the contributions of spurious induced voltage spikes after the inversions. The values reported in Fig. 1f) are the result of the average of 10 inversions.

$$\frac{-\Delta T_{SP}}{j_{e,y}} = (1.19 \pm 0.08) \times 10^{-13}\ \mathrm{Km^2A^{-1}}. \tag{4}$$

Spin Seebeck effect. In the SSE experiment the bulk YIG is the active layer which generates a magnetic moment current when subjected to a temperature gradient, while the Pt is the passive layer in which the injected magnetic moment current is converted into a transverse electric potential. The SSE signal measured across the Pt film $\Delta V_{e,y}$ changes sign when the magnetization of the YIG is inverted in sign (odd parity).

The measurement of the SSE is performed by setting a value of the heat current $I_{q,x}$ traversing the YIG/Pt device and measuring the consequent voltage $\Delta V_{e,y}$ found on the Pt layer when the YIG layer is at magnetic saturation. The set of values obtained $\Delta V_{e,y}$ versus the heat current $I_{q,x}$ is shown in Fig. 1f and a linear fit gives

$$\frac{\Delta V_e}{I_{q,x}} = (2.1 \pm 0.1) \times 10^{-5}\ \mathrm{VW^{-1}} \tag{5}$$

A geometry independent (intrinsic) spin Seebeck coefficient can be defined as $\nabla_y V_e / j_{q,x}$ with $\nabla_y V_e = \Delta V_e / L_{e,y}$ and $j_{q,x} = I_{q,x}/A_q$ with $A_q = L_{e,y} \times L_z$. With $L_{e,y} = 4.17$ mm, the dimension of the Pt electrode used to detect the voltage drop, and $L_z = 3.91$ mm we have

$$\frac{\nabla_y V_e}{j_{q,x}} = (8.2 \pm 0.3) \times 10^{-8}\ \mathrm{VmW^{-1}} \tag{6}$$

Finally the spin Seebeck coefficient $S_{SSE} = \nabla_y V_e / \nabla_x T$, given by the ratio between the transverse gradient of the electric potential $\nabla_y V_e$ in Pt and the longitudinal gradient of the temperature $\nabla_x T$ in YIG (as it is often defined in literature) can be obtained

$$S_{SSE} = -\frac{\nabla_y V_e}{j_{q,x}} \kappa_{YIG} = -(5.4 \pm 0.2) \times 10^{-7}\ \mathrm{VK^{-1}} \tag{7}$$

using the bulk value of the thermal conductivity of YIG: $\kappa_{YIG} = 6.63\ \mathrm{Wm^{-1}\,K^{-1}}$ [32]. This result concurs with another experimental bulk YIG $|S_{SSE}| \simeq 4 \times 10^{-7}\ \mathrm{VK^{-1}}$ [33].

Discussion

The microscopic and physical origin of the spin Peltier and of the spin Seebeck effects has been investigated in det ail[26,28–30,34–43]. These two effects are the results of two independent physical mechanisms. In YIG the presence of a spin current or, more generally, of a magnetic moment current, carried by thermally excited spin waves, is accompanied by a heat current. In Pt the longitudinal spin polarized current is associated with a transverse electric effect due to the inverse spin Hall effect, described by the spin Hall angle θ_{SH}. At the interface between YIG and Pt the spin current is partially injected from one layer into the other[44,45]. By adopting the thermodynamic description of Johnson and Silsbee[46] further developed in refs[21,22,28–30], the thermomagnetic effects in YIG are described by means of the thermomagnetic power coefficient ε_{YIG}, that has an analogous role to the thermoelectric power coefficient ε of thermoelectrics. At the interface, the passage of the magnetic moment current, due to diffusion, is mainly determined by the magnetic moment conductances per unit surface area, ν_M, of the two layers. Basing

on these ideas, it has been possible to work out the reciprocal relation relating the spin Seebeck and spin Peltier effects with the intrinsic and extrinsic parameters of the bilayer. The expression is[21,22]

$$\frac{-\Delta T_{SP}}{j_e}\frac{1}{T} = \frac{\nabla_y V_e}{j_{q,x}} t_{Pt} = \theta_{SH}\mu_0\left(\frac{\mu_B}{e}\right)\frac{1}{\nu_p}\frac{\varepsilon_{YIG}\sigma_{YIG}}{\kappa_{YIG}} \tag{8}$$

Eq. (8) contains two equal signs. The equal sign at the left is between the SPE and SSE measured quantities and we find the temperature difference between the two faces of YIG, ΔT_{SP}, of the SPE generated by the electric current density $j_{e,y}$ and the transverse gradient of the electric potential in Pt, $\nabla_y V_e$, of the SSE, generated by the heat current density, $j_{q,x}$, in YIG. The equal sign at the right refers to the relation of both SPE and SSE to intrinsic coefficients. In addition to the expected parameters: θ_{SH}, the spin Hall angle of Pt and ε_{YIG}, the thermomagnetic power coefficient of YIG, we have: σ_{YIG}, the magnetic moment conductivity of YIG, ν_p, the magnetic moment conductance per unit surface area of the YIG/Pt interface and κ_{YIG}, the thermal conductivity of the YIG. μ_0 is the magnetic constant, μ_B is the Bohr magneton and e is the elementary charge. ν_p depends on the intrinsic conductances, ν_M of both YIG and Pt and on the ratio t/l_M between the thickness t and the magnetic moment diffusion length l_M, for each layer. The expression of ν_p is derived in ref.[22] and reported in the Supplementary material.

By just taking the first equal sign of Eq. (8) and integrating over the size of the bilayer device we have

$$\frac{-\Delta T_{SP}}{I_{e,y}/(L_z \cdot t_{Pt})}\frac{1}{T} = \frac{\Delta V_{e,y}/L_{q,y}}{I_{q,x}/(L_{q,y} \cdot L_z)} t_{Pt} \tag{9}$$

At the left hand side ($L_z \cdot t_{Pt}$) is the area where the electric current flows. At the right hand side ($L_{q,y} \cdot L_z$) is the area of the thermal contact and corresponds to the region where the spin Seebeck effect rises. The previous relation can be simplified, leading to Eq. (1) and permitting a direct test of the reciprocity by using the experimental values. By taking the average temperature $T = (298 \pm 2)$ K, the spin Seebeck experiment gives

$$\frac{\Delta V_{e,y}}{I_{q,x}} T = (6.3 \pm 0.3) \times 10^{-3}\ \mathrm{KA^{-1}} \tag{10}$$

which is in excellent agreement with the spin Peltier value of Eq. (3) and verifies experimentally the reciprocal relation, Eq. (1), between spin Seebeck and spin Peltier effects.

Once the reciprocity is verified, we can take the second equal sign of Eq. (8) and obtain an experimental value that can be compared with the theoretical coefficients. By labeling the value taken from equation (8) as $K_{YIG/Pt}$ we find from the experiments

$$K_{YIG/Pt} = (4.0 \pm 0.3) \times 10^{-16}\ \mathrm{m^2 A^{-1}} \tag{11}$$

We now compare the obtained value with the coefficients known from the literature. For what concerns the spin Hall angle we choose the absolute value of 0.1, similar to what was found experimentally[47,48] on samples of YIG with Pt layers of comparable thickness[49]. In this work we use the spin Hall angle θ_{SH} for the current of magnetic moments which has opposite sign with respect to the one for spin currents reported in the literature (i.e. we have negative θ_{SH} for Pt and positive for W and Ta)[21,22]. By using $\mu_0\sigma_{YIG} = \nu_{YIG} l_{YIG}$ and employing the values of the coefficients determined in previous works[21] ($\varepsilon_{YIG} \simeq -10^{-2}\ \mathrm{TK^{-1}}$ and $\theta_{SH} = -0.1$) we can quantify the only missing parameter, ν_p/ν_{YIG}, as $\nu_p/\nu_{YIG} \simeq 9$. This value is compatible with the transmission of the magnetic moment current between the two layers as determined by the intrinsic diffusion lengths l_M, by the thicknesses t and by the intrinsic conductances ν_M of YIG and Pt. By using the expression for ν_p[22] with $l_{Pt} \simeq 7.3$ nm and $l_{YIG} \sim 0.4\ \mu$m and with $\nu_{YIG} \sim \nu_{Pt}$ we obtain $\nu_p/\nu_{YIG} = 8$ which is reasonably close to the measured value.

We are therefore able to evaluate the cooling potentiality of the spin Peltier effect. If we consider the YIG/Pt device able to operate in adiabatic conditions ($I_{q,c} = 0$), the temperature change across the device ΔT will be

$$\Delta T = \Delta T_{SP} - \mathcal{R}_{YIG} I_{q,JH} \tag{12}$$

where we have assumed $\mathcal{R}_{Pt} \ll \mathcal{R}_{YIG}$ and $\mathcal{R} \simeq \mathcal{R}_{YIG}$. By taking the specific device studied in this paper, the electric current which is maximizing ΔT is $I_{e,y} = -12.4\ \mu$A giving a maximum temperature change of $\Delta T = 3.8 \times 10^{-8}$ K. This value appears so small to discourage any attempt to employ the SPE in practice. However the verification of the validity of the thermodynamic theory for the SPE and SSE (Eq. (8)) offers, in future perspective, the possibility to design and optimize spin Peltier coolers and spin Seebeck generators going beyond the specific bilayer sample used in this experimental study. Work is in progress along this line, however two main preliminary comments are already possible at this stage. The first is to identify the YIG and Pt thicknesses that would optimize the effects. The answer comes from the fact that both materials are active over a thickness of the order of the diffusion length l_M. Therefore promising devices would have $t_{YIG} \sim l_{YIG}$ and $t_{Pt} \sim l_{Pt}$. The second is that, as for thermoelectrics, the thermomagnetic YIG is characterized by a figure of merit $\zeta_T = \varepsilon_{YIG}^2 \sigma_{YIG} T/\kappa_{YIG}$, which is indeed very small at room temperature, $\zeta_T \simeq 4 \times 10^{-3}$[22]. However it is expected that the ζ_T parameter could improve in the temperature range between 50 and 100 K where experiments[50] have reported a much larger SSE (almost a factor 5) than the room temperature value. Finally it is worth to mention that both improvements could further benefit by cascading several devices in thermal series[51]. For example, with $\zeta_T \sim 1$ and using a multilayer with an appropriate compensation of the Joule heat of each layer by using variable cross sections, one could

obtain up to an effective $\Delta T = 20$ K for a device containing ~10^3 junctions. Work along this line has already progressed and future improvements are expected[19].

In summary, we investigated experimentally both the SPE and the SSE in a bulk YIG/Pt device. The thermal observables of these experiments are investigated by means of heat current measurements. This introduces a novel technique for the SPE characterization of a given sample in the DC regime. The experimental results of the SPE and SSE are used to verify for the first time the reciprocal relation between the two. The relation between both effects with the intrinsic and extrinsic parameters of YIG and Pt bilayer offers the possibilities for a more in-depth investigation of the applicability of spincaloritronic devices.

Methods

Device and experimental setup. The YIG/Pt device employed is made of a bulk yttrium iron garnet (YIG) single crystal prepared by crystal growth in high-temperature solutions applying the slow cooling method[52]. Single crystals which nucleate spontaneously at the crucible bottom and grow to several centimetres sizes have been separated from the solution by pouring out the residual liquid. Afterwards, one crystal was cut parallel to one of its facets to prepare slices and parallelepipeds of the following dimensions: $L_y = 4.95$ mm, $L_z = 3.91$ mm, $t_{YIG} = 0.545$ mm. Carefully grinding and polishing result in a sample with optical smooth surfaces ($R_q = 0.4$ nm obtained by AFM). After polishing both sides, a thin film of Pt (t_{Pt} about 5 nm) was sputtered on the top of one of the $L_y \times L_z$ surfaces at University of Loughborough (United Kingdom). Subsequently two 100 nm thick gold electrode strips for electric contacts were deposited. The inner distance between the electrodes is equal to $L_{e,y} = 4.17$ mm. The Au contacts on the Pt layer are electrically connected to 40 μm diameter platinum leads by silver paste. The SSE voltage is measured by means of a Keithley 2182 nanovoltmeter while the SPE electric current is generated by a Keithley 2601 source meter.

In order to avoid heat leakages all measurements are performed under vacuum (1.6×10^{-4} mbar) by means of a turbomolecular pump. The heat current sensors are miniaturized Peltier cells (5×5 mm and 1.9 mm of thickness, RMT Ltd model 1MD04-031-08TEG), calibrated according to the procedure described in ref.[24]. The characteristic $I_q = -S_p V_p$ of both heat sensors are described by $S_p = 0.97 \pm 0.01$ V/W, where I_q is the heat current traversing the sensor and V_p is the voltage measured by a nanovoltmeter. The thermal reservoirs are two brass parallelepipeds ($1 \times 1 \times 2$ cm) to which one face of each heat sensor is glued with silver paste. The other face of each sensor is clamping the YIG/Pt device. We use an aluminum nitride slab ($3 \times 3 \times 4$ mm) with a large nominal thermal conductivity (140–180 $Wm^{-1} K^{-1}$) as geometrical adapter to thermally connect the Pt side of the device with the corresponding heat sensor. Thin layers of silicon based thermal grease are used to ensure uniform thermal conductivity through the sections.

Offset subtractions during SPE and SSE measurements. In the case of the electric current inversion method, the spin Peltier heat signals is affected by a spurious heat current offset, $I_{q,off}$, (a few percent of the total) that is not present in the magnetic field inversion method and should be therefore subtracted. The reason for this spurious heat current offset is that a conventional Peltier effect arises in presence of different metal contacts in the measurement setup (i.e. the contact between Pt and Au layers and the contacts with the electrical leads). These contacts would give a transverse (along y) heat flux, however the presence of an even very small transverse heat leakage may contribute to a small longitudinal contribution. This spurious conventional Peltier effect $I_{q,off}$ presents, with respect to the current inversion, the same odd parity as the spin Peltier signal. When using the odd parity of the SPE under magnetic field inversion the spurious effect is cancelled. Conversely, when determining the SPE through the electric current inversion $\pm I_{e,y}$ method, it is summed up. The offset is subtracted by using one measurement with magnetic field inversion method at saturation as a reference. Also the spin Seebeck experiment is affected by a spurious voltage measured at Pt which is the reciprocal of the one found in the spin Peltier with current inversion. A very small transverse leaking heat flux may gives rise to electric effects in the nV range caused by the ordinary Seebeck effect due to the electric contacts between different metals. Again, this offset voltage is eliminated by using one magnetic field inversion point at saturation as a reference.

Data Availability

All data generated or analysed during this study are included in this published article (and its Supplementary Information files).

References

1. Callen, H. B. *Thermodynamics and an introduction to Thermostatistics* (John Wiley and Sons, New York, 1985).
2. Miller, D. G. Thermodynamics of irreversible processes. The experimental verification of the Onsager reciprocal relations. *Chemical Reviews* **60**, 15–37 (1960).
3. Goldsmid, H. J., Nolas, G. S. & Sharp, J. *Thermoelectrics: basic principles and new materials development* (Springer, Berlin, 2001).
4. Onsager, L. Reciprocal relations in irreversible processes. I. *Physical Review* **37**, 405 (1931).
5. Bauer, G. E. W., Saitoh, E. & van Wees, B. J. Spin caloritronics. *Nature materials* **391**, 11 (2012).
6. Boona, S. R., Myers, R. C. & Heremans, J. P. Spin caloritronics. *Energy Environ. Sci.* **7**, 885 (2014).
7. Yu, H., Brechet, S. D. & Ansermet, J.-P. Spin caloritronics, origin and outlook. *Physics Letters A* **381**, 825–837 (2017).
8. Ansermet, J.-P. Spintronics: Conceptual building blocks. In *et al*., E. B. (ed.) *Magnetism and Synchrotron Radiation, Proceedings in Physics 133*, 43 (Springer, 2010).
9. Yu, X.-Q., Zhu, Z.-G., Su, G. & Jauho, A.-P. Spin-caloritronic batteries. *Phys. Rev. Applied* **8**, 054038 (2017).
10. Martin-Gonzalez, M., Caballero-Calero, O. & Diaz-Chao, P. Nanoengineering thermoelectrics for 21st century: Energy harvesting and other trends in the field. *Renewable and Sustainable Energy Reviews* **24**, 288 (2013).
11. Uchida, K. *et al*. Thermoelectric generation based on spin Seebeck effects. *Proceedings of the IEEE* **104**, 1946 (2016).
12. Dejene, F., Flipse, J. & van Wees, B. Verification of the Thomson-Onsager reciprocity relation for spin caloritronics. *Physical Review B* **90**, 180402 (2014).
13. Flipse, J. *et al*. Observation of the spin Peltier effect for magnetic insulators. *Physical Review Letters* **113**, 027601 (2014).
14. Uchida, K. *et al*. Spin Seebeck insulator. *Nature Materials* **9**, 894 (2010).

15. Uchida, K. *et al*. Observation of longitudinal spin-Seebeck effect in magnetic insulators. *Appl. Phys. Lett.* **97**, 172505 (2010).
16. Uchida, K. *et al*. Longitudinal spin Seebeck effect: from fundamentals to applications. *Journal of Physics: Condensed Matter* **26**, 343202 (2014).
17. Daimon, S., Uchida, K.-I., Iguchi, R., Hioki, T. & Saitoh, E. Thermographic measurements of the spin Peltier effect in metal/yttrium-iron-garnet junction systems. *Phys. Rev. B* **96**, 024424 (2017).
18. Daimon, S., Iguchi, R., Hioki, T., Saitoh, E. & Uchida, K. Thermal imaging of spin Peltier effect. *Nature communications* **7**, 13754 (2016).
19. Uchida, K. *et al*. Enhancement of the spin Peltier effect in multilayers. *Phys. Rev. B* **95**, 184437 (2017).
20. Itoh, R. *et al*. Magnetic-field-induced decrease of the spin Peltier effect in $Pt/Y_3Fe_5O_{12}$ system at room temperature. *Phys. Rev. B* **96**, 184422 (2017).
21. Basso, V. *et al*. Nonequilibrium thermodynamics of the spin Seebeck and spin Peltier effects. *Phys. Rev. B* **93**, 184421 (2016).
22. Basso, V., Kuepferling, M., Sola, A., Ansalone, P. & Pasquale, M. The spin Seebeck and spin Peltier reciprocal relation. *IEEE Magnetics Letters* (2018).
23. Sola, A. *et al*. Evaluation of thermal gradients in longitudinal spin Seebeck effect measurements. *J. Appl. Phys.* **117**, 17C510 (2015).
24. Sola, A. *et al*. Longitudinal spin Seebeck coefficient: heat flux vs. temperature difference method. *Scientific reports* **7**, 46752 (2017).
25. Bougiatioti, P. *et al*. Quantitative disentanglement of the spin Seebeck, proximity-induced, and ferromagnetic-induced anomalous Nernst effect in normal-metal–ferromagnet bilayers. *Physical review letters* **119**, 227205 (2017).
26. Prakash, A. *et al*. Evidence for the role of the magnon energy relaxation length in the spin Seebeck effect. *Physical Review B* **97**, 020408 (2018).
27. Sinova, J., Valenzuela, S. O., Wunderlich, J., Back, C. H. & Jungwirth, T. Spin Hall effects. *Rev. Mod. Phys.* **87**, 1213–1260 (2015).
28. Rezende, S. M., Rodriguez-Suarez, R. L., Cunha, R. O., Ortiz, J. C. L. & Azevedo, A. Bulk magnon spin current theory for the longitudinal spin Seebeck effect. *Journal of Magnetism and Magnetic Materials* **400**, 171–177 (2016).
29. Basso, V., Ferraro, E. & Piazzi, M. Thermodynamic transport theory of spin waves in ferromagnetic insulators. *Phys. Rev. B* **94**, 144422 (2016).
30. Nakata, K., Simon, P. & Loss, D. Spin currents and magnon dynamics in insulating magnets. *Journal of Physics D: Applied Physics* **50**, 114004 (2017).
31. Uchida, K. *et al*. Intrinsic surface magnetic anisotropy in $Y_3Fe_5O_{12}$ as the origin of low-magnetic-field behavior of the spin Seebeck effect. *Physical Review B* **92**, 014415 (2015).
32. Hofmeister, A. M. Thermal diffusivity of garnets at high temperature. *Physics and Chemistry of Minerals* **33**, 45–62 (2006).
33. Uchida, K., Kikkawa, T., Miura, A., Shiomi, J. & Saitoh, E. Quantitative temperature dependence of longitudinal spin Seebeck effect at high temperatures. *Phys. Rev. X* **4**, 041023 (2014).
34. Chotorlishvili, L. *et al*. Fokker-Planck approach to the theory of the magnon-driven spin Seebeck effect. *Phys. Rev. B* **88**, 144429 (2013).
35. Cunha, R. O., Padron-Hernandez, E., Azevedo, A. & Rezende, S. M. Controlling the relaxation of propagating spin waves in yttrium iron garnet/Pt bilayers with thermal gradients. *Phys. Rev. B* **87**, 184401 (2013).
36. Etesami, S. R., Chotorlishvili, L., Sukhov, A. & Berakdar, J. Longitudinal spin current induced by a temperature gradient in a ferromagnetic insulator. *Phys. Rev. B* **90**, 014410 (2014).
37. Rezende, S. M. *et al*. Magnon spin-current theory for the longitudinal spin-Seebeck effect. *Phys. Rev. B* **89**, 014416 (2014).
38. Ritzmann, U. *et al*. Magnetic field control of the spin Seebeck effect. *Phys. Rev. B* **92**, 174411 (2015).
39. Cornelissen, L. J., Peters, K. J. H., Bauer, G. E. W., Duine, R. A. & van Wees, B. J. Magnon spin transport driven by the magnon chemical potential in a magnetic insulator. *Phys. Rev. B* **94**, 014412 (2016).
40. Geprags, S. *et al*. Origin of the spin Seebeck effect in compensated ferrimagnets. *Nat Commun* **7** (2016).
41. Nakata, K., Simon, P. & Loss, D. Wiedemann-Franz law for magnon transport. *Phys. Rev. B* **92**, 134425 (2015).
42. Ohnuma, Y., Matsuo, M. & Maekawa, S. Theory of the spin Peltier effect. *Phys. Rev. B* **96**, 134412 (2017).
43. Saslow, W. M. Irreversible thermodynamics of uniform ferromagnets with spin accumulation: Bulk and interface dynamics. *Phys. Rev. B* **95**, 184407 (2017).
44. Saitoh, E., Ueda, M., Miyajima, H. & Tatara, G. Conversion of spin current into charge current at room temperature: Inverse spin-Hall effect. *Appl. Phys. Lett.* **88**, 182509 (2006).
45. Bender, S. A. & Tserkovnyak, Y. Interfacial spin and heat transfer between metals and magnetic insulators. *Phys. Rev. B* **91**, 140402(R) (2015).
46. Johnson, M. & Silsbee, R. H. Thermodynamic analysis of interfacial transport and of the thermomagnetoelectric system. *Phys. Rev. B* **35**, 4959 (1987).
47. Althammer, M. *et al*. Quantitative study of the spin Hall magnetoresistance in ferromagnetic insulator/normal metal hybrids. *Physical Review B* **87**, 224401 (2013).
48. Wang, H. L. *et al*. Scaling of spin Hall angle in 3d, 4d, and 5d metals from $Y_3Fe_5O_{12}$/metal spin pumping. *Phys. Rev. Lett.* **112**, 197201 (2014).
49. Hoffmann, A. Spin Hall effects in metals. *IEEE transactions on magnetics* **49**, 5172–5193 (2013).
50. Kikkawa, T. *et al*. Critical suppression of spin Seebeck effect by magnetic fields. *Phys. Rev. B* **92**, 064413 (2015).
51. Ramos, R. *et al*. Unconventional scaling and significant enhancement of the spin Seebeck effect in multilayers. *Phys. Rev. B* **92**, 220407 (2015).
52. Görnert, P. & Voigt, F. High temperature solution growth of garnets: theoretical models and experimental results. *Current topics in materials science* **11**, 1–149 (1984).

Acknowledgements

We thank Kelly Morrison at the University of Loughborough for the deposition of the Pt film. We thank Luca Martino and Federica Celegato (from Istituto Nazionale di Ricerca Metrologica) for technical support during the assembling of the measurement system. One author (C.D.) thanks R. Meyer and B. Wenzel for technical support in sample preparation.

Author Contributions

A.S., V.B., M.K. and M.P. devised the measurement technique and wrote the manuscript. C.D. prepared the YIG sample, A.S. developed the measurement setup and characterized the device, V.B. developed the theoretical model. All authors discussed the results, their physical interpretation and reviewed the manuscript.

Additional Information

Supplementary information accompanies this paper at https://doi.org/10.1038/s41598-019-38687-4.

Competing Interests: The authors declare no competing interests.